Supporting Information: Ab Initio Structure Search and in Situ ^{7}Li NMR Studies of Discharge Products in the Li–S Battery System

Kimberly A. See, Michal Leskes, John M. Griffin, Sylvia Britto, Peter D. Matthews, Alexandra Emly, Anton Van der Ven, Dominic S. Wright, Andrew J. Morris,* Clare P. Grey,* and Ram Seshadri*

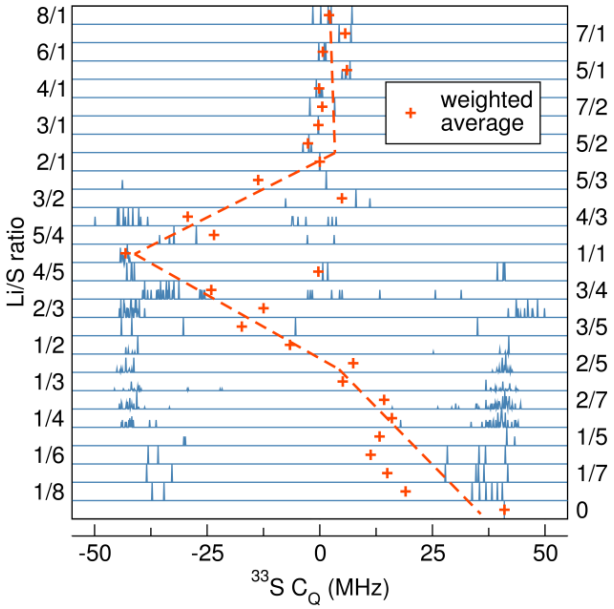

Figure S1. Calculated quadrupolar coupling constants, C_Q, for the ^{33}S nuclei of the low energy compounds in the series Li_xS_{1-x}. The distribution of C_Q values for each S atom in 28 stoichiometries found by AIRSS are shown as histogram plots with the height of the line indicating the number of atoms exhibiting that C_Q. The average ^{33}S C_Q for the averages for the lowest energy compounds are highlighted with a dotted line to assist visualization of structural trends. When the Li/S ratio is over ~2/1 ($x > 0.66$ in Li_xS_{1-x}), the average C_Q value is essentially zero due to the presence of isolated S atoms in relatively symmetric local bonding environments. The average C_Q value then decreases to -40 MHz; this is ascribed to the formation of dumbbells, terminal ^{33}S nuclei in chains and dumbbells exhibiting large negative C_Q values owing to the strong asymmetry of the local bonding environment. A smooth increase in C_Q 40 MHz is then seen as structures which contain increasingly longer chains of S atoms are formed. Internal ^{33}S nuclei within chains, -S-**S**-S-, also have highly asymmetric bonding environments but they exhibit large positive C_Q values (around +40 MHz). The averaged C_Q of these compounds is simply a combination of each S signature with the C_Q weighted appropriately resulting in a gradual increase in C_Q from negative to positive.

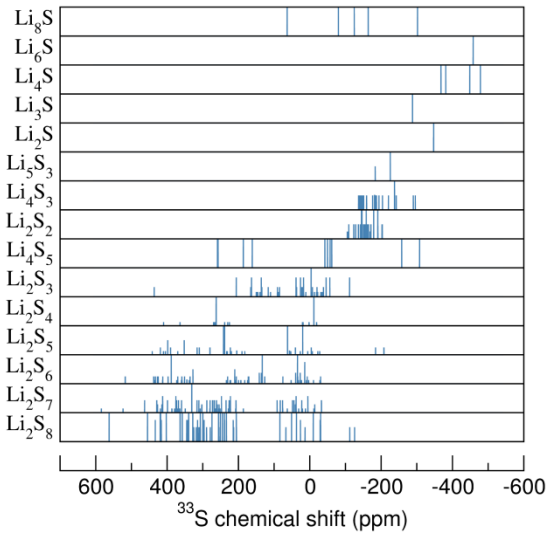

Figure S2. Distributions of calculated resonant frequencies for each ^{33}S nuclei in the low energy compounds in the series of Li_xS_{1-x} displayed as normalized histograms. The values are referenced to Li_2S at -347 ppm.

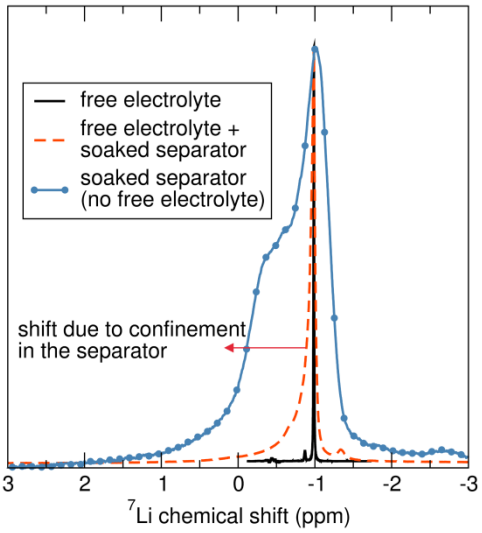

Figure S3. Ex situ ^7Li NMR of the free electrolyte, free electrolyte + a soaked GFD separator, and a soaked GFD separator with no free electrolyte. As the relative percentage of electrolyte confined in the separator increases, a low field component begins to emerge.

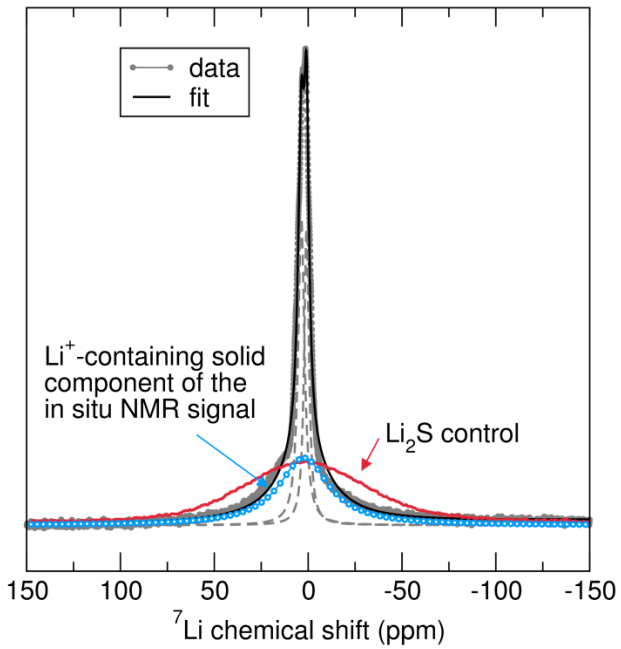

Figure S4. In situ ^{7}Li NMR at the end of discharge (t = 7.2 hr) deconvoluted into 3 components with the Li^{+}-containing solid component highlighted.

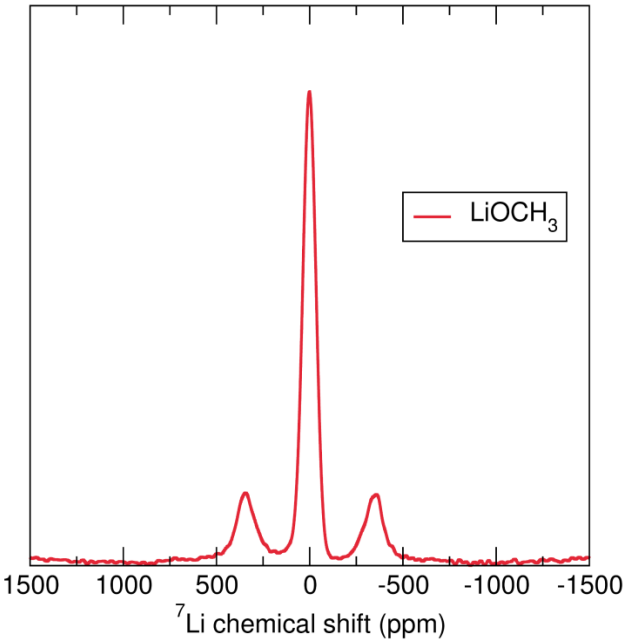

Figure S5. The static ^{7}Li NMR of lithium methoxide ($LiOCH_3$) shows large satellite peaks. The measurement was done on a 300MHz Bruker with a 2 µs 90° pulse (125 kHz excitation) and a relaxation delay of 60 s.

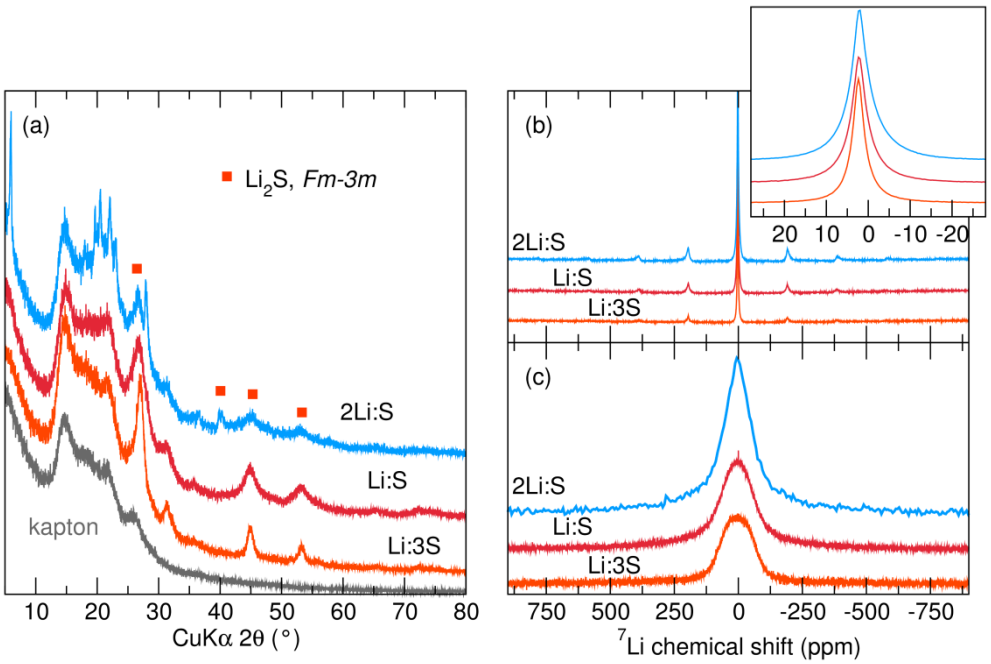

Figure S6. (a) X-ray diffraction patterns (XRD), (b) magic angle spinning solid-state ^{7}Li NMR and (c) static ^{7}Li NMR of three samples prepared by refluxing n-butyl lithium and S_8 at various Li:S ratios in toluene under N_2. The resulting solids were filtered off without exposure to air. XRD was performed between two kapton sheets clamped by an air-sensitive XRD sample holder. The diffractograms were measured on a rotating stage with a Panalytical Empyrean Diffractometer. The NMR rotors were packed in an Ar glove box prior to loading them into the NMR probe. There is no evidence in the XRD pattern or the NMR spectra for the formation of new phases. The peaks between 20-25 2Θ (°) in the 2Li:S sample are likely an organic compound formed due to reaction with the solvent. Additionally, the filtrate was strongly colored suggesting that a significant portion of the S_8 remained in solution. The broadening seen in the static spectrum of the Li:3S sample is ascribed to ^{7}Li-^{7}Li dipolar coupling. On reducing the S content, the resonance sharpens but weak shoulders are seen at high and low frequency of the central component, and the spinning sidebands in the MAS spectrum extend out to higher frequencies. This is ascribed to increased defects within the Li_2S phase/poorer crystallinity (consistent with the XRD); this results in Li environments near defects with non-zero C_Qs (leading to weak sidebands and shoulders from the satellite transitions) and increased mobility of the Li^+ ions, leading to a sharper central component.

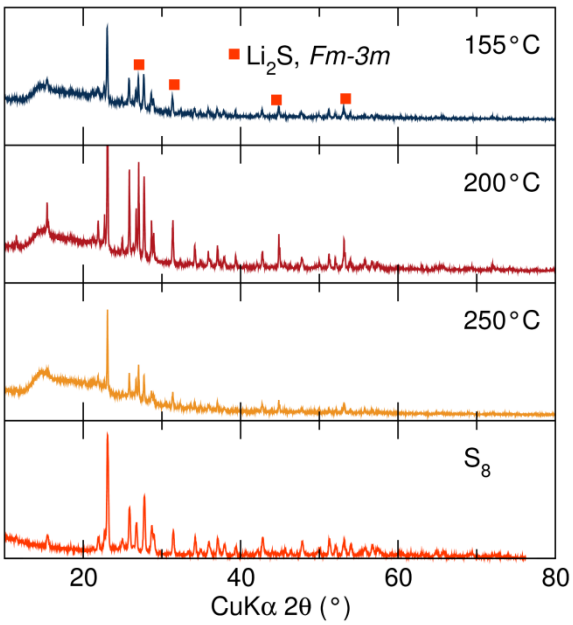

Figure S7. XRD of samples prepared by heating Li_2S and S_8 in a ratio of 2Li:8S in a Parr pressure vessel for 7 hr. at the temperature indicated. The powders were ground with a mortar and pestle prior to loading into the Parr vessel. The powders were loaded inside an Ar glove box in order to maintain an Ar atmosphere inside the Parr. Firstly, the powders were heated to 155°C for 7 hr., the sample was removed and re-ground in an Ar glove box, then heated at the 200°C for 7 hr., and so on. The samples are simply mixtures of S_8 and Li_2S in all instances.

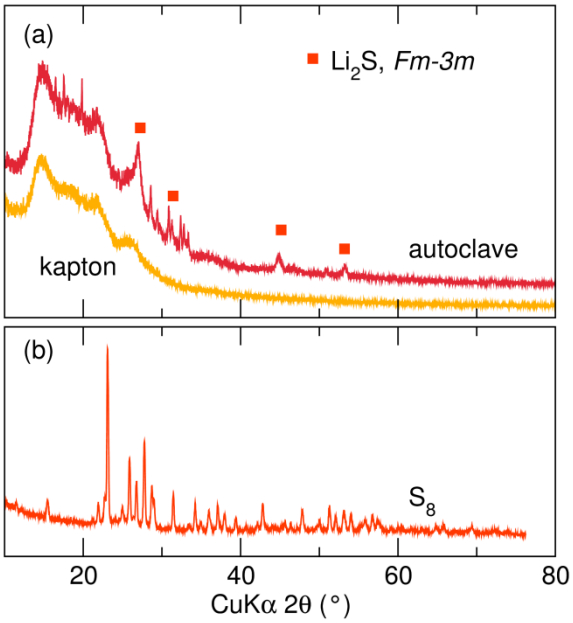

Figure S8. (a) XRD of a 2Li:8S sample prepared by heating n-buLi with S_8 in toluene in an autoclave. The XRD was measured with a kapton air-free sample holder on a rotating stage. The sample is a composite of Li_2S and S_8, shown in (b).

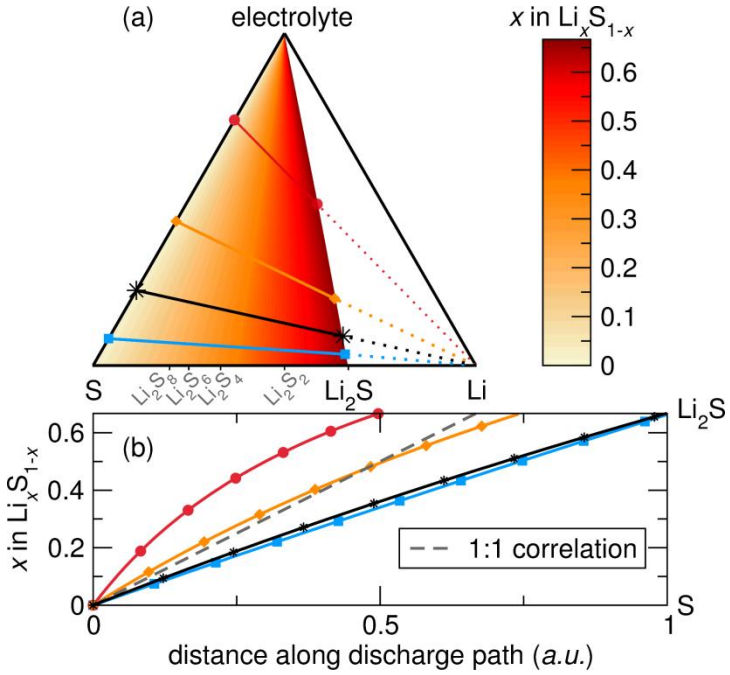

Figure S9. It is important to note that the ternary diagram represents compositions of three phases, however, in a voltage profile, only the Li content is represented on the x-axis (or x in Li_xS_{1-x}). The x-axis, which could be capacity or time, is essentially measuring the number of electrons passed in the cell (for a galvanostatic experiment) which corresponds to the number of Li^+ generated. Therefore, while traveling along the discharge pathway in the ternary, the corresponding lengths of the plateaus in the discharge profile will shrink or stretch depending on the grade of the discharge pathway due to the correlation between x in Li_xS_{1-x} and the location of the discharge pathway in the ternary. (a) The proposed ternary diagram describing the Li-S system with the Li/S ratio present in the phase diagram overlaid as a contour plot. (b) Four possible discharge paths plotted as distance along the path vs. *x* in Li_xS_{1-x} to illustrate how the discharge profile would stretch or shrink depending on the region.